Averaging-Related Biases in Monthly Latent Heat Fluxes

PAUL J. HUGHES AND MARK A. BOURASSA

Department of Earth, Ocean and Atmospheric Science, and Center for Ocean-Atmospheric Prediction Studies, The Florida State University, Tallahassee, Florida

JEREMY J. ROLPH AND SHAWN R. SMITH

Center for Ocean-Atmospheric Prediction Studies, The Florida State University, Tallahassee, Florida

(Manuscript received 5 August 2011, in final form 23 March 2012)

ABSTRACT

Seasonal-to-multidecadal applications that require ocean surface energy fluxes often require accuracies of surface turbulent fluxes to be 5 W m^{-2} or better. While there is little doubt that uncertainties in the flux algorithms and input data can cause considerable errors, the impact of temporal averaging has been more controversial. The biases resulting from using monthly averaged winds, temperatures, and humidities in the bulk aerodynamic formula (i.e., the so-called classical method) to estimate the monthly mean latent heat fluxes are shown to be substantial and spatially varying in a manner that is consistent with most prior work. These averaging-related biases are linked to nonnegligible submonthly covariances between the wind, temperature, and humidity. To provide additional insight into the averaging-related bias, the methodology behind the third-generation Florida State University monthly mean surface flux product (FSU3) is detailed to highlight additional sources of errors in gridded datasets. The FSU3 latent heat fluxes suffer from this averaging-related bias, which can be as large as 90 W m^{-2} in western boundary current regions during winter and can exceed 40 W m^{-2} in synoptically active portions of the tropics. The regional impacts of these biases on the mixed layer temperature tendency are shown to demonstrate that the error resulting from applying the classical method is physically substantial.

1. Introduction

Knowledge of the processes by which energy, moisture, momentum, gases, and matter are transferred across the atmosphere–ocean interface is vital to understanding and predicting climate variability. Direct measurements of these fluxes are sparse in both space and time; therefore, air–sea flux fields derived from indirect methods are needed. Surface flux products based on in situ data [e.g., the third-generation Florida State University monthly mean surface flux product (FSU3) and the National Oceanography Centre Southampton (NOCS) Flux Dataset; see Josey et al. (1999) and Berry and Kent (2009)] are advantageous to climate-related studies because of the long marine meteorological observation record, but the overall applicability is limited by poor and inhomogeneous sampling, along with uncertainties inherent in observations, parameterizations, and the methodology used to derive the flux fields (Gulev et al. 2007a,b). Therefore, the representativeness of the flux estimates depends on how well each of the aforementioned shortcomings is understood and addressed.

One aspect of the methodology that has undergone much scrutiny is the use of the so-called classical method to compute monthly mean turbulent fluxes. In the classical method, the mean fluxes are calculated from the mean meteorological variables; variability on time scales shorter than the averaging period is implicitly neglected. If the shorter time-scale variability (e.g., submonthly) accounts for a large portion of the monthly mean and is not adequately represented in the averaged meteorological variables, then the classical method can introduce a bias into the mean flux estimates (e.g., Budyko 1974; Esbensen and Reynolds 1981; Simmonds and Dix 1989; Gulev 1994, 1997; Josey et al. 1995; Zhang 1995; Esbensen and McPhaden 1996; Simmonds and

Corresponding author address: Paul J. Hughes, 233 RM Johnson Bldg., Center for Ocean-Atmospheric Prediction Studies, The Florida State University, Tallahassee, FL 32306-2840.
E-mail: phughes@fsu.edu

DOI: 10.1175/JTECH-D-11-00184.1

Keay 2002). However, the significance of this bias over the global ocean remains a topic of debate.

This study examines the accuracy of the classical method using 6-hourly 40-yr European Centre for Medium-Range Weather Forecasts (ECMWF) Re-Analysis (ERA-40) data (Uppala et al. 2005) for the period 1978 through 2001. We capitalize on the coverage in time and space of the ERA-40 data to quantify the averaging-related bias in monthly mean latent heat flux estimates over the global ocean. This is done for the following two purposes: 1) to help put differences in past results into better context by obtaining bias estimates in multiple ocean basins and in regions that are poorly sampled by in situ platforms (e.g., outside of major shipping lanes and moored buoy arrays); and 2) to put the magnitude of the bias in perspective with respect to the FSU3 latent heat flux, which was computed using the classical method. The goal is to justify the need for a correction factor that accounts for the averaging-related bias; defining an appropriate correction is beyond the scope of this study. Although this study focuses only on the latent heat flux estimates, the FSU3 sensible heat fluxes will have similar problems because they were derived in the same manner (Smith et al. 2011). We focus on the latent heat flux because it is a major component of the surface energy budget over the ocean, and past studies (e.g., Josey et al. 1995; Gulev 1997) found the latent heat flux biases to be, on average, significantly greater than those associated with the sensible heat flux.

Because gridded flux products have many sources of errors in addition to the averaging method, an overview of the FSU3 development is detailed in section 2, which includes a description of the data that were used to generate the fields (section 2a), the bias corrections (section 2b), the quality control procedures (section 2c), and the objective method (section 2d). Section 2d also provides details about the FSU3 flux calculations, which are pertinent to the subsequent sections that discuss the accuracy of the classical method. The difference between the classical method and an alternative approach, known as the sampling method, is formulated in section 3. The error resulting from applying the classical method is quantified for the latent heat flux in section 4, and is shown to be linked to both the variability of physical processes and the dependence of the transfer coefficient on wind speed and atmospheric stability. In section 5, the physical implications of the averaging-related error are examined in terms of the mixed layer temperature tendency, which shows that the error resulting from applying the classical method on a monthly time scale is substantial for many applications.

2. Overview of FSU3 development

FSU3 is objectively created from in situ ship and buoy observations using release 2.2 of the International Comprehensive Ocean–Atmosphere Data Set (ICOADS; Woodruff et al. 1987; Worley et al. 2005). Monthly fields of wind stress ($\boldsymbol{\tau}$), latent heat flux (E), sensible heat flux (H), pseudostress ($\boldsymbol{\Psi}$), scalar wind speed (w), specific humidity (q), and air temperature (AT) are available on a $1^\circ \times 1^\circ$ spatial grid for the period 1978–2004. Because of the sparsity of in situ data in the Southern Hemisphere, fields are not produced poleward of 30°S. The air–sea fluxes are estimated using the bulk aerodynamic formulas [section 2d(2)]; therefore, the accuracy of the monthly fields is dependent on the quality of the source data, the parameterization of the transfer coefficients, the averaging method, and the objective method. To understand the influence of the averaging method on the overall accuracy, the source data, bias corrections, quality control procedures, objective method, and flux calculations are detailed.

a. Source data

The ICOADS dataset is constructed with historical marine data obtained from a multitude of sources (e.g., merchant ships, fishing vessels, moored buoys, and drifting buoys). The marine data in ICOADS are typically observed at 3–6-h intervals, with more recent reports occurring hourly (mostly from buoys). The individual observations (e.g., air temperature, sea level pressure, specific humidity, and wind speed) are binned on a $1^\circ \times 1^\circ$ grid, and a monthly mean is computed for each variable in each grid box with data. Buoy reports are averaged into daily observations prior to determining the number of observations per month because the hourly data lack independence. Prior to the binning process the individual observations are corrected for known systematic errors (section 2b) and outliers are removed using a quality control procedure (section 2c).

The National Meteorological Center's (NMC's) blended sea surface temperature (SST) analysis (referred to as the Reynolds SSTs hereafter; Reynolds 1988), rather than the ICOADS SSTs, is used to compute the surface turbulent fluxes in the FSU3 product as part of the variational method (section 2d). Reynolds SSTs are constructed from both in situ (ship and buoy) and satellite data, and are used because bias corrections for ship-based SSTs are not well understood and vary greatly from ship to ship.

b. Bias corrections

Prior to the calculation of the FSU3 wind stress and surface turbulent heat fluxes, known systematic errors are removed from the data. Air temperature measurements

from voluntary observing ships (VOS) and buoys are known to contain systematic biases associated with the heating of the vessel's infrastructure and instruments by solar radiation (Berry et al. 2004). To compute surface fluxes to within 10 W m^{-2}, the air temperature should be measured to an accuracy of ±0.2°C (Taylor 2000). The error in air temperature measurements associated with solar heating can be greater than 0.2°C and larger than the air–sea temperature difference, resulting in inaccurate surface flux calculations (Berry et al. 2004). Because the sensible heat flux is directly dependent on the air–sea temperature difference, the bias in air temperature can produce an unrealistic transfer of heat. In addition, the momentum and turbulent heat fluxes are also dependent on the atmospheric stability through the transfer coefficients; therefore, unrealistic stable or near-neutral conditions caused by the air temperature error can result in a reduction of the surface fluxes. To remove the radiative heating errors from the VOS observations in the most severely impacted regions (with very low monthly mean wind speeds), a heat budget model developed by Berry et al. (2004) was applied to the individual ship observations.

The Reynolds SSTs represent a bulk temperature (i.e., the temperature at a depth of the order of 1 m). Because the surface turbulent fluxes are regulated by the interaction of the ocean surface and overlying atmospheric conditions, the Reynolds SSTs are adjusted to represent a skin temperature (i.e., temperature at a depth of <1 mm). The skin temperature is estimated by adding the mean bias of +0.3°C (Donlon and Robinson 1997) to the monthly mean Reynolds SSTs. The authors acknowledge that the bias presented by Donlon and Robinson (1997) includes substantial variability, which is largely a function of time-varying wind speed and downwelling solar radiation (Gentemann et al. 2009). The ICOADS dataset does not provide appropriate observations to accurately determine radiative fluxes, and the winds and solar radiation are far from constant on a monthly scale; therefore, we do not attempt to account for this variability. The monthly average error in latent heat flux resulting from this variability (Weihs 2012) is small compared to the averaging-related error.

The anemometer wind speed observations are height adjusted to a standard height of 10 m using a surface flux model (Bourassa et al. 1999). Ship anemometer observations are presumed to correspond to a constant 20-m reference height. The assumption of a constant ship anemometer height does not remove the spurious upward trend in the height-adjusted winds associated with increasing measurement heights with time (Thomas et al. 2008). The detailed metadata required to accurately adjust the height of the majority of ship wind speed observations were not readily available when the FSU3 was produced.

c. Quality control

Three quality control procedures are implemented to remove erroneous and nonrepresentative observations from the source data for the FSU3. The first quality control procedure is applied to the individual observations, whereas the remaining two are implemented on the monthly mean gridded observational fields.

First, the individual observations are compared to climatological values. Individual marine reports that fall outside 3.5 standard deviations from the da Silva climatology (da Silva et al. 1994) are eliminated. In addition, a minimum standard deviation for each variable is also imposed because of the limited variability of the da Silva climatology in certain regions of the globe (Bourassa et al. 2005). This comparison removes very few observations, and most of those are grossly inconsistent with nearby observations. Visual inspection of monthly data coverage maps for the 27 years of data revealed that no clusters of data have been removed, indicating that this comparison has not caused excessive trimming.

The second quality control procedure, termed "autoflag," flags and removes monthly averaged values at grid points that differ too much from adjacent points. The autoflag routine computes differences between up to eight neighboring nonland 1° grid boxes for each scalar variable—air temperature, sea surface temperature, specific humidity, scalar wind speed, and u and v pseudostress components. Differences in adjacent grid boxes are (on average) larger in regions with greater natural variability. Local monthly variabilities are estimated as the standard deviations of a 5-yr average (e.g., 1999–2003) of 6-hourly ERA-40 reanalyses. The absolute value of each gridcell difference in averaged gridded ship data is divided by the square root of the ERA-40 standard deviation to account for regional variability. The adjusted differences for the whole ocean basin are ordered by magnitude, and the grid boxes associated with the top 3% receive flags. A datum is removed (set equal to a designated missing value) on the basis of the total number of flags a particular grid box receives for that variable. Air temperature, sea surface temperature, and specific humidity are removed (on a variable by variable basis) if a grid box contains five or more flags (out of a possible eight) for that variable. Wind speed data are removed if a grid box contains four or more flags. Last, if three or more of the scalar variables in an individual grid box are set to missing, then all input data values are set to the designated missing value for that grid cell.

Visual comparison of the gridded data from before and after the application of the autoflag test was conducted

to verify that the approach did not remove clusters of data. The FSU3 fluxes are the first version of the FSU winds to employ the autoflag technique. Doing so has reduced the human component of processing time by approximately a factor of 10.

The third quality control procedure uses a graphical user interface developed to display the monthly mean gridded ship and buoy observations. An analyst visually inspects the monthly in situ fields and subjectively removes suspect data that were not eliminated by the preceding quality control methods. The edits are largely made in data-sparse regions, where the autoflag procedure cannot be applied effectively. Very few data are removed in this step, which, not being automated, is the most time intensive.

d. Objective method

A variational method is used to create a gridded analysis of the surface turbulent fluxes and forcing meteorological variables. The analysis is determined by minimizing a cost function, which incorporates both observational and background constraints (Pegion et al. 2000), using a conjugate-gradient minimization scheme (Shanno and Phua 1980). Here the optimal solution is one that best fits the observations (in a least squares sense) while being smooth with respect to the background field. Pegion et al. (2000) found that the background constraints were effective in removing spurious features (e.g., satellite tracks) from the analysis with a minimal amount of smoothing.

Here the cost function (F, see the appendix) is the sum of the cost function (f) at each grid point; f takes the general form

$$f = f_o + f_{\mathrm{bg}}, \tag{1}$$

where f is the total cost function, f_o comprises the observational constraints, and f_{bg} encompasses the background constraints. The observation and background cost functions (f_o and f_{bg}) are defined, respectively, as

$$\begin{aligned} f_o = {} & \beta_{\Psi_s} f_{\Psi_s} + \beta_{\Psi_m} f_{\Psi_m} + \beta_{\Psi_d} f_{\Psi_d} \\ & + \beta_{\mathrm{AT}_s} f_{\mathrm{AT}_s} + \beta_{\mathrm{AT}_m} f_{\mathrm{AT}_m} + \beta_{q_s} f_{q_s} \\ & + \beta_{q_m} f_{q_m} + \beta_{w_s} f_{w_s} + \beta_{w_m} f_{w_m} \end{aligned} \tag{2}$$

and

$$\begin{aligned} f_{\mathrm{bg}} = {} & \beta_{\Psi_{\mathrm{Lap}}} f_{\Psi_{\mathrm{Lap}}} + \beta_{\Psi_{\mathrm{curl}}} f_{\Psi_{\mathrm{curl}}} + \beta_{\mathrm{AT}_{\mathrm{Lap}}} f_{\mathrm{AT}_{\mathrm{Lap}}} \\ & + \beta_{q_{\mathrm{Lap}}} f_{q_{\mathrm{Lap}}} + \beta_{w_{\mathrm{Lap}}} f_{w_{\mathrm{Lap}}} + \beta_{\tau_{\mathrm{Lap}}} f_{\tau_{\mathrm{Lap}}} + \beta_{\tau_{\mathrm{curl}}} f_{\tau_{\mathrm{curl}}} \\ & + \beta_{H_{\mathrm{Lap}}} f_{H_{\mathrm{Lap}}} + \beta_{E_{\mathrm{Lap}}} f_{E_{\mathrm{Lap}}}. \end{aligned} \tag{3}$$

In (2), the fs are the observational constraints, which measure the difference between the solution field and the various types of observations. The s, m, and d in the subscripts represent ship, moored buoy, and drifting buoy observations, respectively. The variables AT, q, and w are the air temperature, specific humidity, and scalar wind speed at a height of 10 m, respectively. Note that at the time of FSU3 production the variables AT, q, and w were not measured by drifting buoys. The pseudostress ($\boldsymbol{\Psi}$) is computed using the observed wind vector components [defined in section 2d(2)]. The wind stress ($\boldsymbol{\tau}$), sensible heat flux (H), and latent heat flux (E) are not directly observed, but are estimated using the bulk aerodynamic formulas using meteorological observations [section 2d(2)].

In (3), the fs represent the background constraints, which operate to ensure spatial continuity of the analysis field. The Lap and curl in the subscripts distinguish the two types of background constraints that are applied—a Laplacian smoothing with respect to the background field and a misfit to the curl of the background field, respectively [see section 2d(1)]. The weights (βs) control the amount of influence each constraint has on the final analysis and are determined using cross validation (Wahba and Wendelberger 1980; Pegion et al. 2000) prior to the minimization of the cost function. The complete cost function is detailed in the appendix.

1) BACKGROUND FIELDS

The background fields are derived from the monthly mean gridded observational fields. Using individual monthly averages was found to be more effective than using a long-term climatology (Bourassa et al. 2005). A Gaussian-weighted spatial average is applied to the in situ monthly fields to determine the background values at each grid point. The weight is a function of the distance, measured in units of grid cells, away from the grid point of interest. The spatial averaging is dependent on the total number of observations: a minimum of 15 observations is required, but a minimum of 100 is desired. However, for specific humidity and air temperature, 100 observations are required near the equator, gradually dropping to 25 at approximately ±38°. Humidity observations at higher latitudes are relatively sparse; therefore, requiring 100 observations would force too much spatial smoothing. The increase in sampling-related errors was considered a lesser problem than the oversmoothing. In areas containing an inadequate number of observations the search radius is increased by one grid cell until a desired number is obtained or a maximum search area is exceeded. The search area in the open ocean is bound by a lower limit and an upper limit, 5 and 11 grid cells, respectively. In the few regions

where the minimum observation requirement is not satisfied the background field is determined by averaging neighboring values of the background field in a creeping fill (Kara et al. 2007). A "line of sight" constraint prohibits data associated with considerably differing regimes (e.g., the Atlantic Ocean and the Mediterranean Sea) from being included in the Gaussian spatial averaging procedure (Bourassa et al. 2005). This restriction permits only observations that have a line of sight that is free of land to be used in determining a value in the background field.

2) Flux calculations

The latent heat flux, sensible heat flux, and wind stress are estimated using the bulk aerodynamic formulas

$$E = \rho L_v C_E w \Delta q, \tag{4}$$

$$H = \rho c_p C_H w \Delta T, \tag{5}$$

$$\boldsymbol{\tau} = \rho C_D \boldsymbol{\Psi}, \tag{6}$$

where ρ is the density of moist air, L_v is the latent heat of vaporization, c_p is the specific heat of air, C_E is the moisture transfer coefficient, C_H is the heat transfer coefficient, C_D is the drag coefficient, Δq is the air–sea humidity difference ($q_{\text{sfc}} - q$), and ΔT is the air–sea potential temperature difference (SST − AT). The variable q_{sfc} represents 98% of the saturation specific humidity corresponding to the sea surface temperature (Reynolds SSTs). The zonal (Ψ_x) and meridional (Ψ_y) components of the pseudostress are defined as

$$\Psi_x = uw, \tag{7}$$

$$\Psi_y = vw, \tag{8}$$

where u and v represent the zonal and meridional components of the wind vector, respectively.

The transfer coefficients, adapted from Bourassa (2006), are similar to the Clayson et al. (1996) parameterizations for C_E and C_H that are based on surface renewal theory. These parameterizations for C_E and C_H are dependent on the boundary layer stratification [parameterized as in Bourassa et al. (1999)] and are largely a function of w and ΔT (dependency on Δq is much weaker). The drag coefficient has a weaker dependence on temperature and humidity, and a much stronger dependence on wind speed. Our C_D is not described in detail here because it does not directly influence the turbulent heat fluxes.

The dependence of our C_E and C_H on w, Δq, and ΔT is advantageous because each variable is expected to change in a covarying manner on the local synoptic scale. Many early forms (e.g., Smith 1980; Large and Pond 1982) of the moisture and heat transfer coefficients have either a simple or negligible dependence on Δq and ΔT, which would result in an unrealistically small sensitivity to changes in the moisture and temperature values.

The monthly mean turbulent fluxes in the FSU3 are estimated by applying Eqs. (4)–(6) to the monthly averaged meteorological variables (i.e., the classical method). Figure 1 shows the climatological annual and seasonal FSU3 latent heat flux fields for the period 1978–2004. The large-scale spatial patterns are generally in agreement with other climatologies; however, the magnitude of the FSU3 latent heat flux was found to be consistently less than other monthly air–sea flux products (Smith et al. 2011). The climatological FSU3 latent heat fluxes are shown here primarily to compare with later results (sections 4 and 5); the reader is directed to Smith et al. (2011) for a more comprehensive look at the FSU3 fields (e.g., latent heat flux, sensible heat flux, momentum flux, and forcing variables) as compared to eight other flux products.

3. Averaging method

In the classical method, Eqs. (4)–(6) are applied to the monthly averaged meteorological variables. An alternative approach, known as the sampling method, applies Eqs. (4)–(6) to the individual meteorological variables, and the mean fluxes are calculated by averaging the individual estimates in a given period. For latent heat flux, the relationship between the two methods is shown by decomposing the right-hand side of (4) into mean and time-varying perturbation components, assuming that L_v is constant and the perturbation in density is negligible,

$$\overline{E} = \overline{\rho} L_v \Bigg(\underbrace{\overline{C_E}\,\overline{w}\,\overline{\Delta q}}_{1} + \underbrace{\overline{C_E}\,\overline{w'\Delta q'}}_{2} + \underbrace{\overline{w}\,\overline{C'_E \Delta q'}}_{3} + \underbrace{\overline{C'_E w'}\,\overline{\Delta q}}_{4} + \underbrace{\overline{C'_E w' \Delta q'}}_{5} \Bigg). \tag{9}$$

The difference between the sampling and classical estimate results from the covariance terms 2–5. Term 2 is largely dependent on the nature of the physical processes (e.g., transient cyclones) that fluctuate on time scales shorter than the averaging period. Terms 3–5 are more dependent on the parameterization of the transfer coefficient (i.e., the sensitivity of C_E to changes in w, Δq, and ΔT). Our C_E is a weak function of Δq and is largely dependent on ΔT [refer to section 2d(2)], which is correlated with synoptic-scale changes in w and q. The sum of terms 2–5 in (9) is an error in the classical approach and will be quantified in section 4.

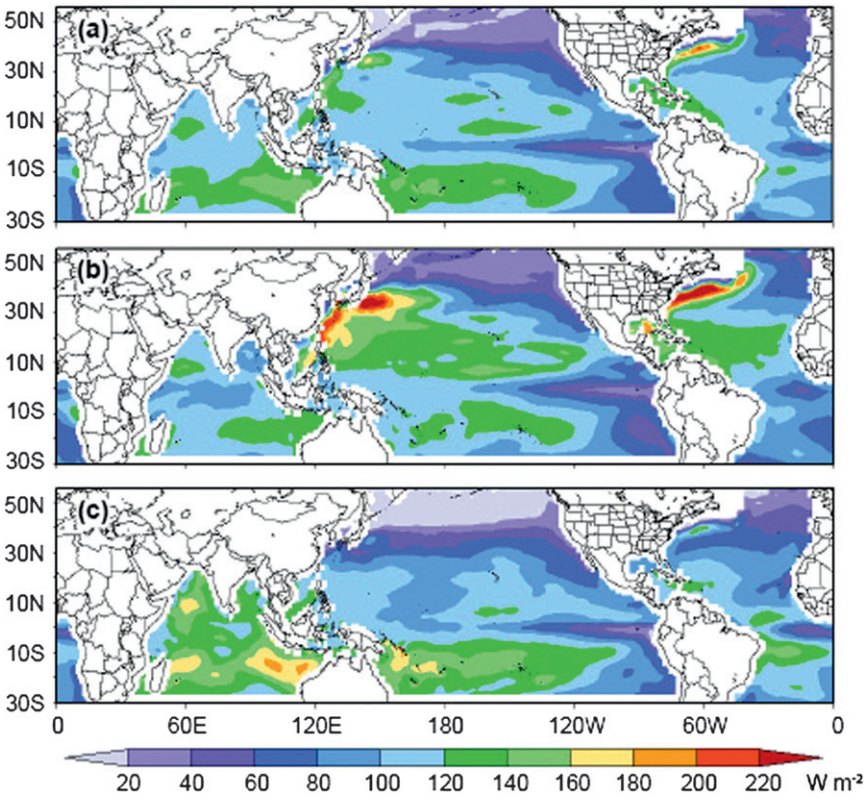

FIG. 1. Climatological (a) annual, (b) December–February, and (c) June–August FSU3 latent heat flux (W m^{-2}) for 1978–2004. Because of the sparsity of in situ data in the Southern Hemisphere, FSU3 fields are not produced poleward of 30°S.

Note that the FSU3 pseudostress does not suffer from this averaging-related problem because (7) and (8) are calculated from individual wind observations prior to averaging. The wind stress (6) is affected, to a lesser extent than the turbulent heat fluxes, through C_D, which has a relatively weak correlation with pseudostress.

4. Quantifying submonthly variability

Quantifying the importance of the covariance terms (globally) is important to the development of new flux climatologies and the application of existing products because these derived fields are used to study climate variability (e.g., in comparison to climate model runs) and to force ocean models. Previous studies have reached conflicting conclusions regarding the accuracy of the classical method. For example, Gulev (1997) found that sampling estimates of the latent and sensible heat fluxes generally give 10%–60% higher values than do classical estimates. Josey et al. (1995) showed opposite results: the sampling latent heat fluxes underestimate classical values by about 10%. Esbensen and Reynolds (1981), Simmonds and Dix (1989), Zhang (1995), and Esbensen and McPhaden (1996) found sampling and classical estimates of the latent and sensible heat fluxes to be in general agreement. Direct comparison and assessment of past results is extremely difficult because of the differing data, time periods, regions, and parameterizations of the transfer coefficients used.

In this study, the differences between sampling and classical monthly mean latent heat flux estimates are investigated using 6-hourly ERA-40 data for the period 1978 through 2001. Reanalyses offer complete and consistent coverage in time and space over the global ocean, and will help to put past results into better context. For example, Esbensen and Reynolds (1981) and Josey et al. (1995) used data from ocean weather ships. Although ocean weather ships provide temporally dense (i.e., either hourly or 3-hourly reports) and long records, the data are point observations. Therefore, the results based on point observations are greatly dependent on the weather conditions throughout the observing period at a specific location and may not be representative of broader or remote regions. This point was acknowledged by Josey et al. (1995), who stated that at other locations their findings may be reversed (i.e., a classical mean that underestimates the sampling value). The use of reanalysis data may help to connect the observational studies to larger areas, making

the results more applicable. However, the surface variables in the reanalyses are not free from sampling problems. In well-sampled regions the reanalysis fields are strongly constrained by the observations; however, in poorly sampled areas the fields are largely governed by the atmospheric model (Gulev et al. 2007a). Therefore, our results depend on the quantity and quality of assimilated observations (Bengtsson et al. 2004). Other inherent problems in the reanalysis meteorological fields [e.g., ERA-40's representation of the hydrological cycle; see Uppala et al. (2005) and Dee et al. (2011)] can influence our results, especially if the problems are inconsistent in time.

Here sampling latent heat fluxes are computed by applying (4) to the 6-hourly ERA-40 atmospheric data and then averaging over the individual estimates for a given month. The consistent nature of the surface variables in the reanalyses (i.e., coincident in space and time) is ideal for the sampling method because no interpolation is needed to the compute the fluxes. The classical estimates are calculated by applying (4) to the monthly averaged ERA-40 atmospheric variables. The climatological annual cycle of the sampling minus classical differences is shown in Fig. 2. The main features are (i) the classical method substantially underestimates the sampling estimate by an amount that is dependent on season, and (ii) the mean differences are not negligible in the tropics.

The largest sampling minus classical differences are generally found in the midlatitudes (Fig. 2), where the bias can represent a large fraction (>40%) of the FSU3 latent heat flux estimate (Fig. 1). In the North Atlantic and Pacific midlatitudes, the bias exhibits a pronounced annual cycle; maximum values, on average, vary from 20 to 30 W m^{-2} in July to greater than 90 W m^{-2} in January (Fig. 2). During the boreal winter, early spring, and late autumn, the bias also shows a clear zonal inhomogeneity; larger sampling minus classical differences are located in the western ocean basins near the continental margins. The spatial and temporal characteristics of the bias in the North Atlantic and Pacific midlatitudes are linked to changes in the synoptic-scale variability associated with transient cyclones (Cayan 1992a,b; Josey et al. 1995; Gulev 1997; Simmonds and Keay 2002).

In the western ocean basins, especially near the continental margins and SST fronts, high positive correlations occur in the cold sectors of midlatitudinal cyclones between the vertical temperature and humidity gradients and wind speed (Gulev 1997). Therefore, term 2 in (9) contributes extensively to the large sampling minus classical differences in the western North Atlantic and Pacific midlatitudes during the boreal winter, early spring, and late autumn (Fig. 2).

In the eastern North Atlantic midlatitudes, Josey et al. (1995) and Gulev (1997) found term 2 to be negative; the weather conditions tend to favor moist air at high wind speeds and dry air at low wind speeds. Therefore, to get positive sampling minus classical differences in the eastern North Atlantic and Pacific midlatitudes (Fig. 2), terms 3–5 in (9) must be cumulatively positive and greater in magnitude than term 2. Because our C_E is weakly dependent on wind speed, term 3 is expected to be largely responsible for the positive sampling minus classical differences in the eastern basins. This is in contrast to the results of Gulev (1997), Esbensen and Reynolds (1981), Simmonds and Dix (1989), and Josey et al. (1995). Gulev (1997), who found similar sampling minus classical differences to ours, showed that term 4 has the most significant impact on the latent heat flux estimate in the northeastern Atlantic. Esbensen and Reynolds (1981), Simmonds and Dix (1989), and Josey et al. (1995) found terms 3–5 in (9) to be cumulatively negligible for specific locations in the eastern North Atlantic and Pacific midlatitudes. Therefore, the accuracy of the classical method in the eastern North Atlantic and Pacific midlatitudes is highly dependent on the parameterization of C_E.

In the tropics, the sampling minus classical differences are generally <10 W m^{-2} [consistent with the findings of Simmonds and Dix (1989), Zhang (1995), Esbensen and McPhaden (1996), and Gulev (1997)], which can represent approximately 10%–20% of the FSU3 latent heat flux (Fig. 1). Although relatively small, the bias still can be physically substantial compared to the 5 W m^{-2} desired accuracy (e.g., Webster and Lukas 1992; Weller et al. 2004) specified from Tropical Ocean and Global Atmosphere Coupled Ocean–Atmosphere Response Experiment (TOGA COARE). Larger sampling minus classical differences are found in regions of increased atmospheric variability (e.g., ITCZ, western Pacific warm pool, and Indian monsoon), where the bias, on average, can be as large as 40 W m^{-2} (Fig. 2). In these regions, particularly the ITCZ and western Pacific warm pool, the greater differences can be largely attributed to the wind speed variability (Cayan 1992b; Esbensen and McPhaden 1996); however, changes in Δq cannot be dismissed. Cayan (1992a,b,c) stated that in the tropics latent heat flux anomalies may be forced by changes in SST through its impact on the saturation vapor pressure. On the basis of our formulation of C_E, term 3 in (9) is likely the primary contributor to the positive sampling minus classical differences in the tropics. This is consistent with the findings of Gulev (1997), who also found term 5 (the triple covariance) to be nonnegligible.

5. Implication on mixed layer temperature

Over the ocean, the latent heat flux is a major component of the surface heat budget, especially during the

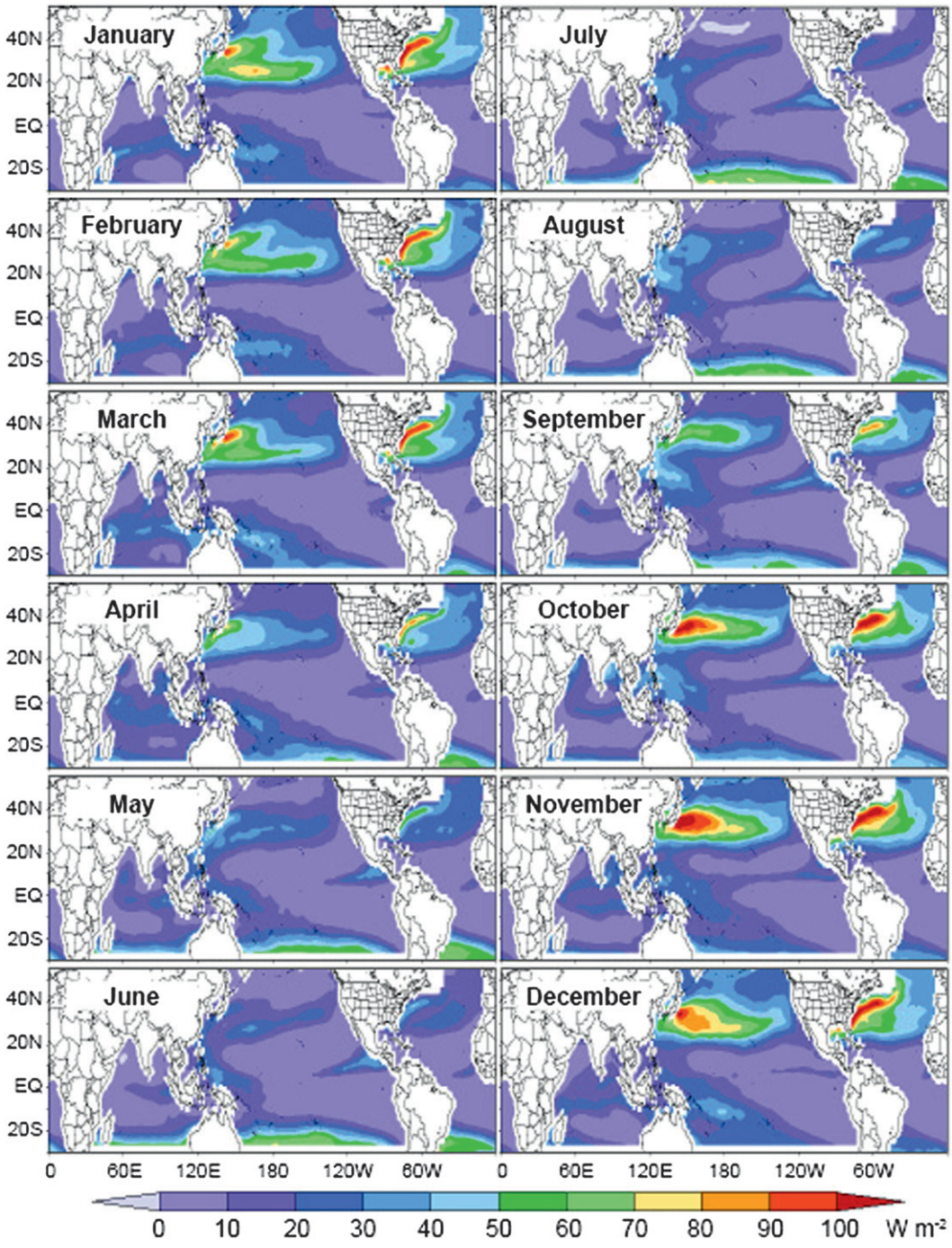

FIG. 2. Estimated climatological monthly bias (W m^{-2}) resulting from implementing the classical time-averaging method. The errors are estimated using 6-hourly ERA-40 data for the period 1978–2001 and interpolated to the FSU3 1° × 1° grid.

winter when much of the heat accumulated in the upper ocean is transferred to the atmosphere. The physical implications of the differences between sampling and classical latent heat flux estimates (Fig. 2) on the upper ocean are examined using a simple one-dimensional model that predicts the tendency of the mixed layer temperature ($\delta T/\delta t$). In this model, the upper ocean is assumed to be a well-mixed slab that exchanges heat with the atmosphere and the effects of horizontal temperature advection, turbulent mixing, and entrainment

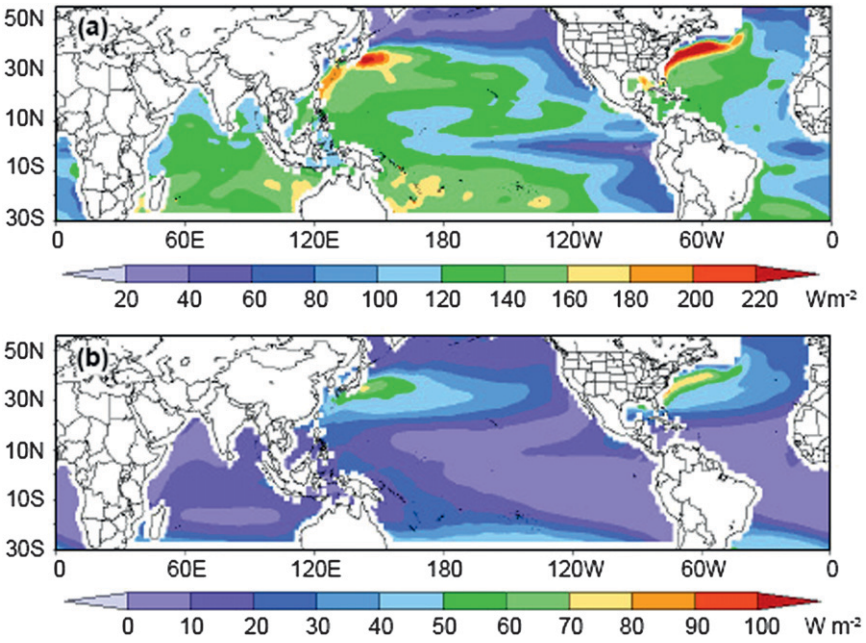

FIG. 3. Climatological annual (a) bias-corrected FSU3 latent heat flux (W m^{-2}) for 1978–2004 and (b) difference. The difference is computed by subtracting the climatological annual FSU3 latent heat flux (Fig. 1a) from the bias-corrected FSU3 latent heat flux.

from below the mixed layer are neglected. Therefore, the change in the mixed layer temperature tendency ($\delta T'/\delta t$) resulting from neglecting the covariance terms in (9) is solely forced by the latent heat flux bias (E_{bias}),

$$\frac{\partial T'}{\partial t} = \frac{-E_{\text{bias}}}{\rho_w C_p h}. \tag{10}$$

Here E_{bias} is the climatological sampling minus classical differences that are shown in Fig. 2, ρ_w is the density of seawater, C_p is the heat capacity, and h is the monthly climatological mixed layer depth (de Boyer Montégut et al. 2004) that was interpolated to the $1° \times 1°$ FSU3 grid.

The latent heat flux bias was positive in all cases, resulting in a greater amount of energy being removed from the ocean. Annually, this difference in the transfer of latent heat can be 10–50 W m^{-2} over much of the midlatitudes (larger values over the Gulf Stream and Kurishio) and portions of the tropics (Fig. 3). Note that (10) is similar to Cayan's (1992c) (3), which was used to relate monthly anomalies of latent and sensible heat fluxes to anomalous SST tendencies. Cayan (1992c) found that the simplified model worked reasonably well over much of the oceans, especially in the extratropics during the cool season. However, near the equator the SST anomalies were found to be more strongly influenced by internal ocean processes rather than by the turbulent heat fluxes (Cayan 1992c).

In general, the largest changes in the mixed layer temperature tendency occur in the North Atlantic and Pacific midlatitudes, where differences can exceed 1°C $month^{-1}$ (Fig. 4). Here the smallest changes occur during the boreal winter, when values generally vary from 0.1 to 0.7°C $month^{-1}$. Differences greater than 1°C $month^{-1}$ are widespread during July–October (Fig. 4) and largely coincide with relatively small latent heat flux biases (e.g., July and August in Fig. 2). This amplified boreal summertime response of the mixed layer temperature tendency to relatively small biases is likely due to the shallower mixed layer depth in the de Boyer Montégut et al. (2004) climatology. A smaller amount of energy is required to change the temperature.

September through November is a transitional period, when the mixed layer depth progressively deepens to its winter maximum and the latent heat flux bias increases. The large changes in mixed layer temperature tendency during this period in the North Atlantic and Pacific midlatitudes (Fig. 4) highlight the importance of accurately representing both surface and subsurface processes for heat budget studies. The same can be said for March–May (Fig. 4), except during this period the mixed layer depth and latent heat flux bias are decreasing. In the tropics, the changes in the mixed layer temperature tendency are largely less than 0.1°C $month^{-1}$; however, in regions of increased oceanic (subsurface) and atmospheric variability (e.g., ITCZ, Indian Ocean monsoon, gap flow, and equatorial Pacific cold tongue), the differences can be substantially greater.

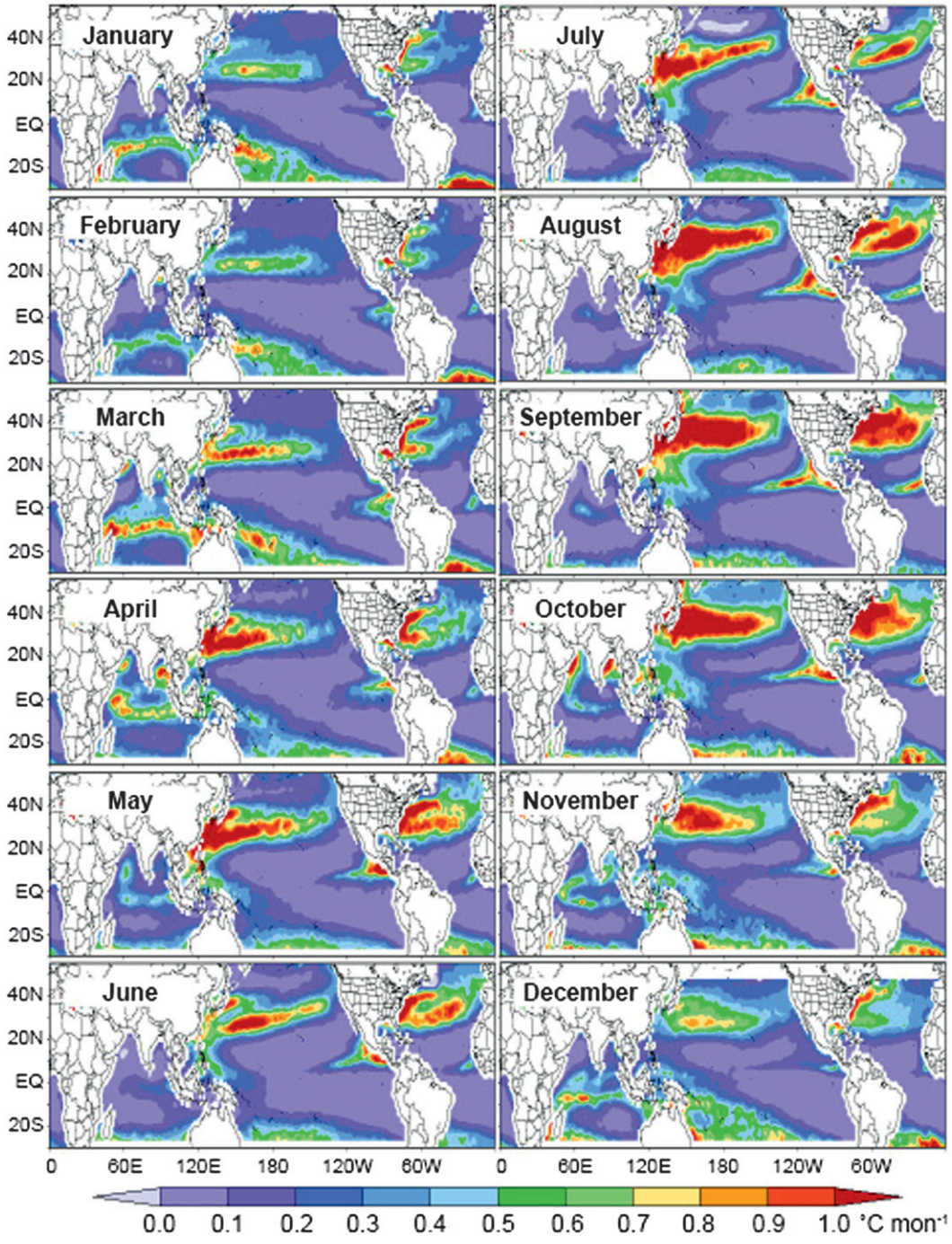

FIG. 4. Climatological monthly difference in the mixed layer temperature tendency (°C month^{-1}) resulting from the latent heat flux bias (Fig. 2) for 1984–2003. The positive values indicate that the latent heat flux bias causes a reduction in the mixed layer temperature tendency.

6. Conclusions

The classical monthly mean latent heat flux is found to substantially underestimate the sampling estimate in both the midlatitudes and tropics. In the Northern Hemisphere midlatitudes and in portions of the tropics (e.g., ITCZ and Indian monsoon), the bias exhibits a pronounced annual cycle. Therefore, in regions of heightened atmospheric variability it is crucial not only to sufficiently capture the shorter time-scale (e.g., synoptic) covariance between the meteorological variables, but also to select a proper transfer coefficient

parameterization (i.e., parameterizations with realistic dependence on wind speed and atmospheric stability) when applying the bulk flux formulas. Failing to do so can greatly diminish the representativeness and applicability of air–sea turbulent flux climatologies. For example, Gulev (1994, 1997) showed that the classical and sampling methods can not only produce very different climatological means and variability for the respective latent and sensible heat fluxes, but also influence the evaluation of key parameters of climate variability that are dependent on these fluxes (e.g., meridional heat transport). Similarly, the authors show that the averaging-related latent heat flux bias can greatly alter the tendency of the mixed layer temperature over midlatitudinal and tropical regions.

The climatological latent heat flux bias that is calculated here is consistent with the findings of Gulev (1997). The results suggest that a correction should be applied to the FSU3 latent and sensible heat fluxes to account for the averaging-related bias, especially in the midlatitudes, before using the product in scientific inquiries. Monthly biases are found to exhibit significant interannual variability in the tropics and midlatitudes (not shown); therefore, it is not recommended that the user correct the FSU3 latent heat fluxes with the estimated mean bias. Note that the FSU3 pseudostress does not suffer from the averaging-related problem and the wind stress is affected to a lesser extent than the turbulent fluxes (refer to section 3).

The purpose of this study is to justify the need for a correction factor. Because of the significance of the climatological monthly bias and interannual variability, further work is needed to (i) examine the dependence of the bias on different reanalysis products (inherent problems in the meteorological variables and differing assimilated data can potentially influence the results), (ii) estimate the individual covariance terms for both the latent and sensible heat fluxes, and (iii) estimate an appropriate monthly correction factor for the FSU3 latent and sensible heat fluxes and any other flux product that uses the classical averaging method on a monthly scale.

In regions that are relatively well sampled (e.g., moored buoy arrays and major shipping lanes), employing the sampling method would improve the accuracy of the derived turbulent flux fields. However, even in these regions the submonthly variability can be inadequately observed because of the point-like sampling characteristics of the in situ platforms. For the satellite era, the combination of in situ and remotely sensed data can help overcome the sampling deficiencies inherent to ships and buoys and improve the representativeness of small-scale features, which will ultimately lead to more accurate turbulent flux climatologies. However, the longevity of the in situ marine meteorological observation record compared to the relatively short satellite data record makes in situ–based turbulent flux products a valuable resource for climate variability and validation applications. Therefore, continued work is needed to reduce in situ observational uncertainties and sampling errors (e.g., through additional marine data rescue) and to develop new techniques that minimize the impact of these errors on derived turbulent flux products.

Acknowledgments. Support for the development of these flux fields and the related science was initially provided by the NSF Division of Ocean Sciences, and support for production and most of the development came from NOAA's Office of Climate Observations in the Climate Observation Division.

APPENDIX

The Cost Function

The complete cost function is written as

$$
F = \sum_{i,j}^{I,J} \left\{ \begin{aligned}
&\beta_{\Psi_s}\sigma_{\Psi_s}^{-2}[(\Psi_{x_a}-\Psi_{x_s})^2-(\Psi_{y_a}-\Psi_{y_s})^2]+\beta_{\Psi_m}\sigma_{\Psi_m}^{-2}[(\Psi_{x_a}-\Psi_{x_m})^2-(\Psi_{y_a}-\Psi_{y_m})^2]\\
&\quad+\beta_{\Psi_d}\sigma_{\Psi_d}^{-2}[(\Psi_{x_a}-\Psi_{x_d})^2-(\Psi_{y_a}-\Psi_{y_d})^2]+\beta_{\Psi_{\mathrm{Lap}}}L^4[\nabla^2(\Psi_{x_a}-\Psi_{x_{\mathrm{bg}}})^2]\\
&\quad+\beta_{\Psi_{\mathrm{Lap}}}L^4[\nabla^2(\Psi_{y_a}-\Psi_{y_{\mathrm{bg}}})^2]+\beta_{\Psi_{\mathrm{curl}}}L^2[\hat{k}\bullet\nabla\times(\boldsymbol{\Psi}_a-\boldsymbol{\Psi}_{\mathrm{bg}})^2]\\
&\quad+\beta_{\mathrm{AT}_s}\sigma_{\mathrm{AT}_s}^{-2}(\mathrm{AT}_a-\mathrm{AT}_s)^2+\beta_{\mathrm{AT}_m}\sigma_{\mathrm{AT}_m}^{-2}(\mathrm{AT}_a-\mathrm{AT}_m)^2\\
&\quad+\beta_{\mathrm{AT}_{\mathrm{Lap}}}L^4[\nabla^2(\mathrm{AT}_a-\mathrm{AT}_{\mathrm{bg}})]^2+\beta_{q_s}\sigma_{q_s}^{-2}[\ln(q_a)-\ln(q_s)]^2\\
&\quad+\beta_{q_m}\sigma_{q_m}^{-2}[\ln(q_a)-\ln(q_m)]^2+\beta_{q_{\mathrm{Lap}}}L^4\{\nabla^2[\ln(q_a)-\ln(q_{\mathrm{bg}})]\}^2\\
&\quad+\beta_{w_s}\sigma_{w_s}^{-2}[\ln(w_a)-\ln(w_s)]^2+\beta_{w_m}\sigma_{w_m}^{-2}[\ln(w_a)-\ln(w_m)]^2\\
&\quad+\beta_{w_{\mathrm{Lap}}}L^4\{\nabla^2[\ln(w_a)-\ln(w_{\mathrm{bg}})]\}^2+\beta_{\tau_{\mathrm{Lap}}}L^4[\nabla^2(\tau_{x_a}-\tau_{x_{\mathrm{bg}}})]^2\\
&\quad+\beta_{\tau_{\mathrm{Lap}}}L^4[\nabla^2(\tau_{y_a}-\tau_{y_{\mathrm{bg}}})]^2+\beta_{\tau_{\mathrm{curl}}}L^2[\hat{k}\bullet\nabla\times(\boldsymbol{\tau}_a-\boldsymbol{\tau}_{\mathrm{bg}})]^2\\
&\quad+\beta_{H_{\mathrm{Lap}}}L^4[\nabla^2(H_a-H_{\mathrm{bg}})]^2+\beta_{E_{\mathrm{Lap}}}L^4[\nabla^2(E_a-E_{\mathrm{bg}})]^2
\end{aligned} \right\}. \tag{A1}
$$

TABLE A1. Objectively determined weights.

Weight	Value of weight
$\beta_{\Psi s}$	1.0
$\beta_{\Psi m}$	20.0
$\beta_{\Psi d}$	0.1
$\beta_{\Psi\mathrm{Lap}}$	0.6
$\beta_{\Psi\mathrm{curl}}$	1.0
$\beta_{\mathrm{AT}s}$	1.0
$\beta_{\mathrm{AT}m}$	0.01
β_{ATLap}	1400.0
β_{qs}	0.008
β_{qm}	0.01
$\beta_{q\mathrm{Lap}}$	6.0
β_{ws}	1.0
β_{wm}	10.0
$\beta_{w\mathrm{Lap}}$	120.0
$\beta_{\tau\mathrm{Lap}}$	1.24
$\beta_{\tau\mathrm{curl}}$	1.2
$\beta_{H\mathrm{Lap}}$	17.3
$\beta_{E\mathrm{Lap}}$	117.8

Here i and j are indices for longitude and latitude, and I and J are the number of longitudinal and latitudinal grid points. The subscript a represents the analysis field and the subscript bg indicates the background field. The subscripts s, m, and d represent ship, moored buoy, and drifting buoy observations, respectively. The βs are objectively determined weights (Table A1), which control the amount of influence each constraint has on the final analysis. The Ls are grid-spacing-dependent length scales that make the cost function nondimensional. The σs are an estimate of local variability (uncertainty squared). The local uncertainty in the observations is estimated from the mean monthly variability based on 6-hourly observations in the National Centers for Environmental Prediction–National Center for Atmospheric Research (NCEP–NCAR) reanalysis (Kalnay et al. 1996)

$$\sigma^2 = \frac{\sigma^2_{\mathrm{NCEP}}}{n}, \tag{A2}$$

where n is the number of ship observations per month. This calculation assumes that sampling variability (insufficient sampling) is the dominant source of error in a monthly average. Comparison to estimates of observational errors, based on the findings of Kent et al. (1998), has shown that this is almost always a good assumption. The uncertainties for the Laplacian (Lap) and curl terms are treated as a global average and are combined with the weights.

REFERENCES

Bengtsson, L., K. I. Hodges, and S. Hagemann, 2004: Sensitivity of the ERA40 reanalysis to the observing system: Determination of the global atmospheric circulation from reduced observations. *Tellus,* **56A,** 456–471.

Berry, D. I., and E. C. Kent, 2009: A new air-sea interaction gridded dataset from ICOADS with uncertainty estimates. *Bull. Amer. Meteor. Soc.,* **90,** 645–656.

——, ——, and P. K. Taylor, 2004: An analytical model of heating errors in marine air temperature for ships. *J. Atmos. Oceanic Technol.,* **21,** 1198–1215.

Bourassa, M. A., 2006: Satellite-based observations of surface turbulent stress during severe weather. *Atmosphere-Ocean Interactions,* Vol. 2, W. Perrie, Ed., Wessex Institute of Technology, 35–52.

——, D. G. Vincent, and W. L. Wood, 1999: A flux parameterization including the effects of capillary waves and sea state. *J. Atmos. Sci.,* **56,** 1123–1139.

——, R. Romero, S. R. Smith, and J. J. O'Brien, 2005: A new FSU winds climatology. *J. Climate,* **18,** 3686–3698.

Budyko, M. I., 1974: *Climate and Life*. International Geophysical Series, Vol. 18, Academic Press, 508 pp.

Cayan, D. R., 1992a: Variability of latent and sensible heat fluxes estimated using bulk formulae. *Atmos.–Ocean,* **30,** 1–42.

——, 1992b: Latent and sensible heat flux anomalies over the northern oceans: The connection to monthly atmospheric circulation. *J. Climate,* **5,** 354–369.

——, 1992c: Latent and sensible heat flux anomalies over the northern oceans: Driving the sea surface temperature. *J. Phys. Oceanogr.,* **22,** 859–881.

Clayson, C. A., C. W. Fairall, and J. A. Curry, 1996: Evaluation of turbulent fluxes at the ocean surface using surface renewal theory. *J. Geophys. Res.,* **101** (C12), 28 503–28 513.

da Silva, A., A. C. Young, and S. Levitus, 1994: *Algorithms and Procedures*. Vol. 1, *Atlas of Surface Marine Data 1994,* NOAA Atlas NESDIS 6, 83 pp.

de Boyer Montégut, C., G. Madec, A. S. Fischer, A. Lazer, and D. Iudicone, 2004: Mixed layer depth over the global ocean: An examination of profile data and a profile-based climatology. *J. Geophys. Res.,* **109,** C12003, doi:10.1029/2004JC002378.

Dee, D. P., and Coauthors, 2011: The ERA-interim reanalysis: Configuration and performance of the data assimilation system. *Quart. J. Roy. Meteor. Soc.,* **137,** 553–597.

Donlon, C. J., and I. S. Robinson, 1997: Observations of the oceanic thermal skin in the Atlantic Ocean. *J. Geophys. Res.,* **102** (C8), 18 585–18 606.

Esbensen, S. K., and R. W. Reynolds, 1981: Estimating monthly averaged air-sea transfers of heat and momentum using the bulk aerodynamic method. *J. Phys. Oceanogr.,* **11,** 457–465.

——, and M. J. McPhaden, 1996: Enhancement of tropical ocean evaporation and sensible heat flux by atmospheric mesoscale systems. *J. Climate,* **9,** 2307–2325.

Gentemann, C. L., P. J. Minnett, and B. Ward, 2009: Profiles of ocean surface heating (POSH): A new model of upper ocean diurnal warming. *J. Geophys. Res.,* **114,** C07017, doi:10.1029/2008JC004825.

Gulev, S. K., 1994: Influence of space–time averaging on the ocean–atmosphere exchange estimates in the North Atlantic midlatitudes. *J. Phys. Oceanogr.,* **24,** 1236–1255.

——, 1997: Climatologically significant effects of space–time averaging in the North Atlantic sea–air heat flux fields. *J. Climate,* **10,** 2743–2763.

——, T. Jung, and E. Ruprecht, 2007a: Estimation of the impact of sampling errors in the VOS observations on air–sea fluxes. Part I: Uncertainties in climate means. *J. Climate,* **20,** 279–301.

——, ——, and ——, 2007b: Estimation of the impact of sampling errors in the VOS observations on air–sea fluxes. Part II: Impact on trends and interannual variability. *J. Climate,* **20,** 302–315.

Josey, S. A., E. C. Kent, and P. K. Taylor, 1995: Seasonal variations between sampling and classical mean turbulent heat flux estimates in the eastern North Atlantic. *Ann. Geophys.,* **13,** 1054–1064.

——, ——, and ——, 1999: New insights into the ocean heat budget closure problem and analysis of the SOC air–sea flux climatology. *J. Climate,* **12,** 2856–2880.

Kalnay, E., and Coauthors, 1996: The NCEP/NCAR 40-Year Reanalysis Project. *Bull. Amer. Meteor. Soc.,* **77,** 437–471.

Kara, A. B., A. J. Wallcraft, and H. E. Hurlburt, 2007: A correction for land contamination of atmospheric variables near land–sea boundaries. *J. Phys. Oceanogr.,* **37,** 803–818.

Kent, E. C., P. K. Taylor, and P. Challenor, 1998: A comparison of ship and scatterometer-derived wind speed data in open ocean and coastal areas. *Int. J. Remote Sens.,* **19,** 3361–3381.

Large, W. G., and S. Pond, 1982: Sensible and latent heat flux measurements over the ocean. *J. Phys. Oceanogr.,* **12,** 464–482.

Pegion, P. J., M. A. Bourassa, D. M. Legler, and J. J. O'Brien, 2000: Objectively derived daily ''winds'' from satellite scatterometer data. *Mon. Wea. Rev.,* **128,** 3150–3168.

Reynolds, R. W., 1988: A real-time global sea surface temperature analysis. *J. Climate,* **1,** 75–86.

Shanno, D. F., and K. H. Phua, 1980: Remark on algorithm 500—A variable method subroutine for unconstrained nonlinear minimization. *ACM Trans. Math. Software,* **6,** 618–622.

Simmonds, I., and M. Dix, 1989: The use of mean atmospheric parameters in the calculation of modeled mean surface heat fluxes over the world's oceans. *J. Phys. Oceanogr.,* **19,** 205–215.

——, and K. Keay, 2002: Surface fluxes of momentum and mechanical energy over the North Pacific and North Atlantic Oceans. *Meteor. Atmos. Phys.,* **80,** 1–18.

Smith, S. D., 1980: Wind stress and heat flux over the ocean in gale force winds. *J. Phys. Oceanogr.,* **10,** 709–726.

Smith, S. R., P. J. Hughes, and M. A. Bourassa, 2011: A comparison of nine monthly air–sea flux products. *Int. J. Climatol.,* **31,** 1002–1027, doi:10.1002/joc.2225.

Taylor, P. K., Ed., 2000: Intercomparison and validation of ocean-atmosphere energy flux fields. Joint WCRP/SCOR Working Group on Air–Sea Fluxes (SCOR Working Group 110) Final Rep., WMO/TD 1036, 306 pp. [Available online at http://eprints.soton.ac.uk/69522/.]

Thomas, B. R., E. C. Kent, V. R. Swail, and D. I. Berry, 2008: Trends in ship wind speeds adjusted for observation method and height. *Int. J. Climatol.,* **28,** 747–763.

Uppala, S. M., and Coauthors, 2005: The ERA-40 Re-Analysis. *Quart. J. Roy. Meteor. Soc.,* **131,** 2961–3012.

Wahba, G., and J. Wendelberger, 1980: Some new mathematical methods for variational objective analysis using splines and cross-validation. *Mon. Wea. Rev.,* **108,** 1122–1143.

Webster, P. J., and R. Lukas, 1992: TOGA COARE: The Coupled Ocean-Atmosphere Response Experiment. *Bull. Amer. Meteor. Soc.,* **73,** 1377–1416.

Weihs, R., 2012: Modeled diurnally varying sea surface temperatures on surface heat fluxes. M.S. thesis, Dept. of Earth, Ocean, and Atmospheric Science, The Florida State University, 46 pp. [Available from FSU ETD, 600 W. College Ave., Tallahassee, FL 32306.]

Weller, R. A., F. Bradley, and R. Lukas, 2004: The interface or air–sea flux component of the TOGA Coupled Ocean–Atmosphere Response Experiment and its impact on subsequent air–sea interaction studies. *J. Atmos. Oceanic Technol.,* **21,** 223–257.

Woodruff, S. D., R. J. Slutz, R. L. Jenne, and P. M. Steurer, 1987: A Comprehensive Ocean–Atmosphere Data Set. *Bull. Amer. Meteor. Soc.,* **68,** 1239–1250.

Worley, S. J., S. D. Woodruff, R. W. Reynolds, S. J. Lubker, and N. Lott, 2005: ICOADS Release 2.1 data and products. *Int. J. Climatol.,* **25,** 823–842.

Zhang, G. J., 1995: Use of monthly mean data to compute surface turbulent fluxes in the tropical Pacific. *J. Climate,* **8,** 3084–3090.